Physical Imaging of Bone Sequential Light Microscopy Observations

Elisa Budyn, Julien Jonvaux, Thierry Hoc

CSMA 2011
10e Colloque National en Calcul des Structures
9-13 Mai 2011, Presqu'île de Giens (Var)

Physical Imaging of Bone Sequential Light Microscopy Observations

E. Budyn[1], J. Jonvaux[1], T. Hoc[2]

[1] *Department of Mechanical Engineering, University of Illinois at Chicago, USA, {ebudyn,jjonva2}@uic.edu*
[2] *LTDS CNRS UMR 5513, Ecole Centrale Lyon, France thierry.hoc@ec-lyon.fr*

Résumé — We propose to evaluate the precision of Digital Image Correlation applied to sequential light microscopy observations of fracturing human Haversian cortical bone. The displacement field on the surface of 3D samples is tracked using a cross-correlation formulation. Due to the potential high number of sequential observations, this study focuses on evaluating displacements at a given growth step obtained either by "direct" comparison of the studied step and the undeformed initial state or by "gradual" comparisons of successive pairs of observations. Due to bone high heterogeneity, two types of correlation procedures are considered with or without domain partition (WDP or WODP) delimiting material and strong discontinuities.
Mots clés — digital image correlation, imaging, fracture, toughness, contact, bone.

1 Introduction

As imaging biological tissues is known to be challenging due to their complex microstructures and mechanical behavior, specific procedures are required in particular when microcracks appear. In the particular case of human Haversian cortical bone failure, microfractures can be studied in micro mechanical tests where small growing cracks are imaged by light microscopy. The experimental setting to monitor and characterise bone micro cracks is implemented in a miniaturised compression device adapted to 3D millimetric samples placed under a light microscope. The test generates numerous surface observations at successive loading steps. Between sequential observations, the displacements of a set of discrete grid points is measured by Digital Image Correlation (DIC). DIC techniques intend to match analogous pixel domains in a reference and a deformed images by minimising a coefficient of correlation either directly between an initial and the considered observations or gradually between successive pairs of images in procedures denoted "direct" or "gradual" correlations respectively. In the gradual procedure, two cases are also studied denoted "invariant gradual correlation" and "varying gradual correlation". For invariant gradual correlation, the successive deformation gradients of the initial correlation domain build a composite deformation function. In this case the correlation is performed on an invariant domain throughout the sequence of images. For varying gradual correlation, the correlation domain between two successive images is always set circular in the first image of the pair. The correlation domain then varies between the first and last images of the sequence.

The cross-correlation formulation, denoted "CC", is applied for the correlation between grey-level intensities [1] first at a sungle pixel precision and the at the subpixel precision is achieved by means of a gradient-based descent algorithm [2] that is reliable for large grey-level discontinuities and using full optimisation [3, 4, 2, 5, 6]. The displacements are measured using a zero-centered normalised cross-correlation formulation that suppresses differences in average luminosity and contrast between the reference and the deformed observations :

$$C^k = 1 - \frac{\displaystyle\sum_{i\in(\Omega_c^k,\omega_c^k)} \left(f(\mathbf{X}_i) - \overline{f}_{\Omega_c^k}\right)\left(g(\mathbf{x}_i) - \overline{g}_{\omega_c^k}\right)}{\sqrt{\displaystyle\sum_{i\in\Omega_c^k}\left(f(\mathbf{X}_i) - \overline{f}_{\Omega_c^k}\right)^2}\sqrt{\displaystyle\sum_{i\in\omega_c^k}\left(g(\mathbf{x}_i) - \overline{g}_{\omega_c^k}\right)^2}} \tag{1}$$

where $\mathbf{X}_i$ and $\mathbf{x}_i$ are the pixel/subpixel coordinates of a point i in the reference picture S_0 and the deformed picture S_n respectively. f and g are the grey-level of pixel/subpixel i in S_0 and S_n respectively. $\overline{f}_{\Omega_c^k}$ and $\overline{g}_{\omega_c^k}$ are the average grey-levels on the correlation domain in S_0 and S_n respectively.

In each correlation domain centered at the studied set of points, the local displacement field is most commonly assumed linear in two dimensions [7, 8, 9, 10] and the local deformations homogeneous. As the constitutive behaviors of biological tissues are typically difficult to characterise [11, 12], the inclusion of *a priori* formulations tied to idealised defects can often misrepresent the physics of the material. Therefore preliminary investigations of an unknown biology is often guided by simplified models in well-identified localised regions [13]. Nonetheless the definition of the correlation domain can sometimes be complemented by a careful description of the tissue morphology denoted “with domain partition" (WDP) in Fig. 2. When the microstructure is not explicit in the correlation domain, the method is denoted “without domain partition" (WODP) in Fig. 1. Both procedures are presented for their respective qualities.

WODP method is used when osteonal lamellae discontinuities are neglected considering that osteonal lamellae are composed of intricated mineralised fibers of which the varying orientations form material phases of limited stiffness contrast (less than 1.5). At points near Haversian canals, where the hollowed regions are included in both the reference and deformed images, one can opt for no domain partition as the correlation coefficient is expected to reasonably calculate the projection between similar grey-level domains. However for points near microcracks or strong discontinuities generating high stress concentration, WODP is expected to be imprecise. The correlation at these points is then achieved by a linear interpolation between the corners of a triangle containing $\underline{X}_0^k$. This triangle should be located on the crack side and in the material phase of $\underline{X}_0^k$ and its corners are manually selected in the reference and deformed images.

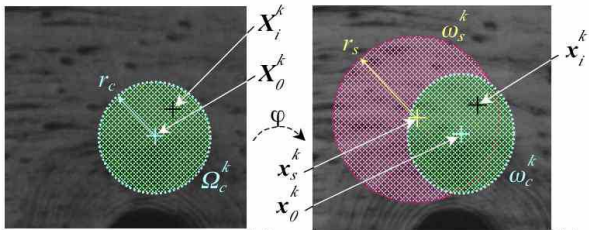

FIG. 1 – WODP Method : (a) zoom of the reference picture S_0 showing point i of coordinates $\underline{X}_i^k$ in the reference correlation domain Ω_c^k of radius r_c and center $\underline{X}_0^k$, (b) zoom of the deformed picture S_n ($n = 4$) showing the deformed correlation domain ω_c^k of center $\underline{x}_0^k$ located in the search domain ω_s^k of radius r_s and centered at $\underline{x}_s^k$

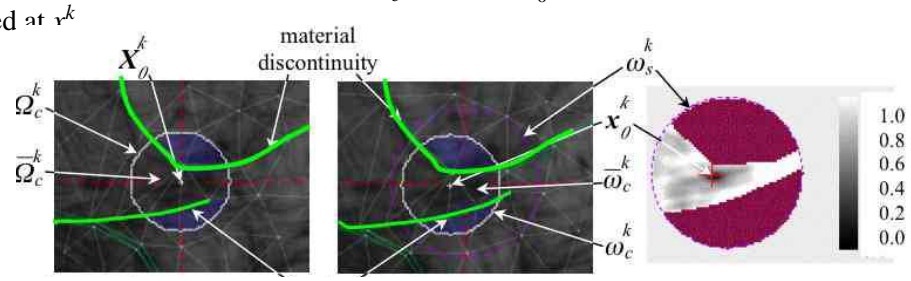

FIG. 2 – WDP method : (a) zoom of the reference picture S_0 showing the correlation domain Ω_c^k of radius r_c and center $\underline{X}_0^k$ and the effective correlation domain $\bar{\Omega}_c^k$ delimited by a crack and a material discontinuity, (b) zoom of the deformed picture S_n ($n = 4$) showing the correlation domain ω_c^k of center $\underline{x}_0^k$ located in the search domain ω_s^k of radius r_s and centered at $\underline{x}_s^k$; $\bar{\omega}_c^k$ is the effective correlation domain. (c) Correlation coefficient field in ω_s^k.

WDP method is applied when no type of discontinuities (osteonal lamellae, Haversian canals, cracks) is neglected, the correlation is performed between effective and homeomorphic correlation domains $\bar{\Omega}_c^k$ and $\bar{\omega}_c^k$ in the same material phase in Fig. 2. The reference and deformed domains Ω_c^k and ω_c^k are partitioned into sub-regions $\Omega_{c(in)}^k$ and $\omega_{c(in)}^k$ around $\underline{X}_0^k$ and $\underline{x}_0^k$ in the same materials and on the same crack side. When crack c does not pass through but has its tip in Ω_c^k, a virtual extension is considered up to the closest discontinuity or the boundary of Ω_c^k. We also check that $\underline{X}_0^k$ is inside a material phase and that the size of $\Omega_{c(in)}^k$ is sufficient. In the deformed image, $\omega_{c(in)}^k$ is determined around point $\underline{x}_0^k$ to locate the pixels in the same material phase as $\underline{X}_0^k$ and on the same crack side as $\underline{x}_0^k$, or on the same crack side as $\underline{X}_0^k$ if a crack is stationary or grows straight. Therefore, the correlation is performed between the effective

correlation domains in the reference and deformed observations that are defined by :

$$\bar{\Omega}_c^k = \Omega_{c(in)}^k \cap \underline{\varphi}^{-1}(\omega_{c(in)}^k) \tag{2a}$$

$$\bar{\omega}_c^k = \underline{\varphi}\left(\bar{\Omega}_c^k\right) = \underline{\varphi}\left(\Omega_{c(in)}^k\right) \cap \omega_{c(in)}^k \tag{2b}$$

The final registration of the points is determined when the correlation satisfies :

1. a threshold criterion where C_k must be less than a set value,
2. the verification of the existence of a strong minimum in the correlation field in Fig. 2,
3. a visual inspection of the point location.

In Haversian cortical bone observations, few points are considered either "wrong" or "unreliable". The "unreliable" points, n_u, are defined as points at which the correlation carries *a priori* high uncertainties despite possibly satisfying the above criteria. These areas are typically regions outside the material boundaries like holes, zones containing a growing phase such as water, damaged surfaces with low contrast, unlevelled areas with poor focus, but also sheared or cracked areas in WODP correlation and cement lines in WDP correlation respectively. The "wrong" points, n_w, are defined as points that are not unreliable but where the correlation procedure returns an aberrant match. At these points the displacements will also further be visually measured. All the points that are neither unreliable nor wrong are called "automatic" and denoted $\underline{u}^{auto}$.

To evaluate the precision of the automatic displacements calculated by correlation methods that verify the above registration criteria and typically 1, it is customary to generate synthetic "simulated" images by assigning known theoretical displacements called $\underline{u}^{theo}$ (chosen linear here) to the image pixels. However in experimental biological images, no analytical displacement field is known. Nonetheless to compare direct and gradual cross-correlations, a "reference experimental field" called $\underline{u}^{visu}$ is visually assessed in the deformed image with single pixel precision only and assumed to be the closest target pixel in the deformed image corresponding to a studied pixel in the initial image. The points of $\underline{u}^{visu}$ are called "visually registered" and are also the default displacement measurement at tagged points when all correlation methods have failed.

Furthermore these digital discrete displacement measurements can contribute to analyse bone failure when a consistent mechanical model includes these microscopic data as essential boundary conditions of a finite element interpolation [14]. The ultimate purpose of Digital Image Correlation in biological tissues that generate large data set, is to visualise the kinematic field as accurately as possible at any location within the tissue based on information that can only be collected at a discrete point set for efficiency. However in these tissues, the discrete displacement field $\underline{u}_k$ determined by DIC at n_g grid points is representative of the real kinematics $\underline{u}_k^{theo}$ provided that the biological morphology and mechanics are incorporated into the correlation method. Therefore when discrete information are collected, the continuous interpolated displacement is also representative provided that the same local morphology and tissue mechanics are included into the interpolation scheme to be consistent with the DIC method.

As a preliminary approach to investigate the mechanical behavior of cortical bone which exhibits a very complex microstructure, we consider a simplified mechanical model in a refined morphology, which is consistent with the DIC field approximation. First the n_g discrete points at which the correlation is measured must be in sufficient number and at relevant locations when the correlation assumes local homogeneous deformations. Second the interpolation scheme must remain consistent with the imaging description to faithfully reconstruct a continuous field based on the n_g displacements by applying a finite element method (FEM) in the framework of linear elasticity and small deformations. To be coherent with WDP methods accounting polyphase domains, the biological microstructure needs to be explicit. Moreover the morphology discretisation counteracts some limitations of WODP methods. The bone discretisation contains n_n FEM nodes defining a set $\mathcal{M}$ conforming to the polyphase biomaterial. Because bone morphological partition is directly consistent with a local partition of the mechanical behavior, the interpolation of the displacement field at any point in $\mathcal{M}$ should include the explicit morphology and the mechanical heterogeneity to become more representative. The linearly interpolated displacement denoted

$\underline{u}^{fem}$ can be calculated at any location $\underline{X}$ by the following equation :

$$\underline{u}^{fem}(\underline{X}) = \sum_{I=1}^{n_n} N_I(\underline{X})\underline{u}_I^{fem} \qquad \forall I \in \mathcal{M} \tag{3}$$

where N_I are the shape functions of the FEM discretisation based on the n_n points For interpolation purposes, the displacement determined by DIC at the n_g points can be applied as essential boundary conditions of the FEM model at a set of nodes $\mathcal{N}_g$ inserted in $\mathcal{M}$ by nodal adaptivity. The FEM displacement solved at all nodes in $\mathcal{M}$ appears then consistent with the phase morphology and mechanics introduced in WDP correlation while WODP tends to average multiple phase contributions.

2 Methodology

The grid of $n_g = 12 \times 10 = 120$ points is laid over the cortical bone sample image in the anti-plane longitudinal direction of observation.The displacements are calculated using three cross-correlation methods denoted "CC" between undeformed state S_0 and final deformed state S_4 ($n = 4$).

The methods are first tested in images of a controlled type with a known theoretical linear displacement field [15], denoted "simulated". The image size is $2048 \times 2048 px^2$ and of microscopic scale $1.48 \mu m\, px^{-1}$.

The correlations methods are then applied experimental images exhibit a high heterogeneous nature that includes material phases of complex constitutive behavior, Haversian canals, microcracks for which no analytical displacement field is known.

In order to compare the accuracy between correlation methods, two indicators are calculated :
- a first indicator is the average difference in displacements between correlation methods and theoretical values (simulated images) or visual measurements (experimental observations) ;
- a second indicator is the interpolated field from the discrete information at n_g points using morphological and material data. The difference of interpolated fields deriving from correlations and theoretical/visual values are presented.

3 Results

Discontinuous displacement difference at the DIC grid points : the first indicator of accuracy studies the difference between automatic displacements calculated by a correlation method and theoretical/visual measurement at each grid point as follows :

$$\Delta\underline{u}_k = \underline{u}_k^{auto} - \underline{u}_k^{theo} \tag{4}$$

where $\underline{u}_k^{auto}$ is the automatic displacement of point k calculated by a correlation method and $\underline{u}_k^{theo}$ is the known theoretical displacement at point k that is prescribed in simulated images. In experimental images $\Delta\underline{u}_k$ is expressed by :

$$\Delta\underline{u}_k = \underline{u}_k^{auto} - \underline{u}_k^{visu} \tag{5}$$

where $\underline{u}_k^{visu}$ is the displacement of single pixel precision at point k that is visually measured. The norm of the displacement difference $\|\Delta\underline{u}\|$ is calculated for the automatic points at the exclusion of the wrong or unreliable points. For direct and gradual cross-correlations, $\|\Delta\underline{u}_k\|$ at point k is defined by :

$$\|\Delta\underline{u}_k\| = \sqrt{(\underline{u}_{k_x}^{auto} - \underline{u}_{k_x}^{visu})^2 + (\underline{u}_{k_y}^{auto} - \underline{u}_{k_y}^{visu})^2} \tag{6}$$

The average of norm of the displacement difference $\overline{\|\Delta\underline{u}\|}$ is also defined by :

$$\overline{\|\Delta\underline{u}\|} = \frac{1}{n_a}\sum_{k=1}^{n_a} \|\Delta\underline{u}_k\| \tag{7}$$

with $n_a = n_g - (n_w + n_u)$ are the automatic displacements. The results are presented in Tab. 1 for simulated images and in Tab. 2 for experimental observations. To compare the proportion of $\overline{\|\underline{\Delta u}\|}$ values to a common average displacement, a normalised average displacement difference is defined by :

$$N_{\underline{\Delta u}} = \frac{\overline{\|\underline{\Delta u}\|}}{\overline{\|\underline{u}\|}} \tag{8}$$

where $\overline{\|\underline{u}\|}$ is defined by :

$$\overline{\|\underline{u}\|} = \frac{1}{n_m} \sum_{i=1}^{n_m} \|\underline{u}_i^{theo/visu}\| \tag{9}$$

where n_m is the number of "measured" points that contains the automatic and visually measured points substituted to all wrong points and few unreliable points that are located in a material phase as well as the points in sheared or cracked areas in WODP correlation and in cement lines in WDP correlation.

TAB. 1 – Average displacement differences $\overline{\Delta u_x}$, $\overline{\Delta u_y}$, $\overline{\|\Delta u\|}$ (px) and normalised average displacement differences $N_{\underline{\Delta u}}$ $(\%)$ with their standard deviations for WODP correlation methods in simulated images.

Method	$\overline{\Delta u_x}$ (px)	$\overline{\Delta u_y}$ (px)	$\overline{\|\Delta u\|}$ (px)	$N_{\underline{\Delta u}}$ $(\%)$
Direct CC	.0058 (.0338)	.00002 (.0604)	.0586 (.0371)	.274
Invariant Gradual CC	.0070 (.1428)	.0057 (.1189)	.1652 (.0842)	.774
Varying Gradual CC	.0059 (.1367)	.0124 (.1194)	.1599 (.0858)	.749

TAB. 2 – Average displacement differences and their standard deviations for WODP and WDP correlation methods in experimental images. The numbers of unreliable, wrong and visually measured points are indicated.

	Method	$\overline{\Delta u_x}$ (px)	$\overline{\Delta u_y}$ (px)	$\overline{\|\Delta u\|}$ (px)	$N_{\underline{\Delta u}}$ $(\%)$	Unreliable points	Wrong points	Visual points
WODP	Direct CC	$-.293$ (.643)	.030 (.581)	.737 (.538)	.842	14	8	17
	Invariant Gradual CC	.288 (.663)	$-.056$ (.589)	.745 (.559)	.851	14	2	11
	Varying Gradual CC	.291 (.669)	$-.057$ (.604)	.765 (.556)	.874	14	2	11
WDP	Direct CC	$-.239$ (.695)	.010 (.714)	.840 (.581)	.959	12	3	5
	Invariant Gradual CC	.321 (.790)	.037 (.695)	.902 (.625)	1.031	12	1	1
	Varying Gradual CC	.308 (.799)	.020 (.682)	.895 (.625)	1.022	12	1	1

Continuous interpolated FEM displacement difference : the second indicator studies the interpolated displacement field from the discrete information at n_g points enhanced by morphological and material data. The difference of interpolated displacement fields deriving from correlations and theoretical/visual values. Fig. 3 and 4 presents normalised difference of interpolated displacement fields in the experimental images defined at point I by :

$$N^{fem}_{\Delta\underline{u}_I} = \frac{\|\underline{\Delta u}^{fem}_I\|}{\sqrt{\frac{\int_\Omega \|\underline{u}^{fem}\|^2 d\Omega}{\int_\Omega d\Omega}}} \times 100 \tag{10}$$

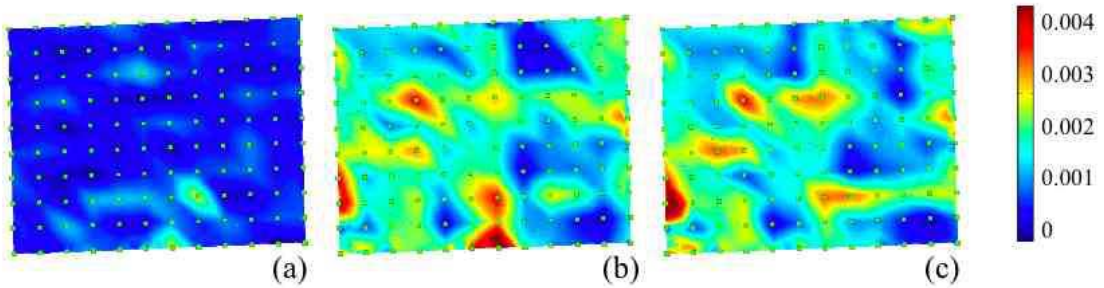

FIG. 3 – Mappings of normalised errors in displacement $N^{fem}_{\Delta\underline{u}_I}$ as defined in Eq. 10 in simulated images for (a) a direct cross-correlation, (b) an invariant gradual cross-correlation and (c) a varying gradual cross-correlation.

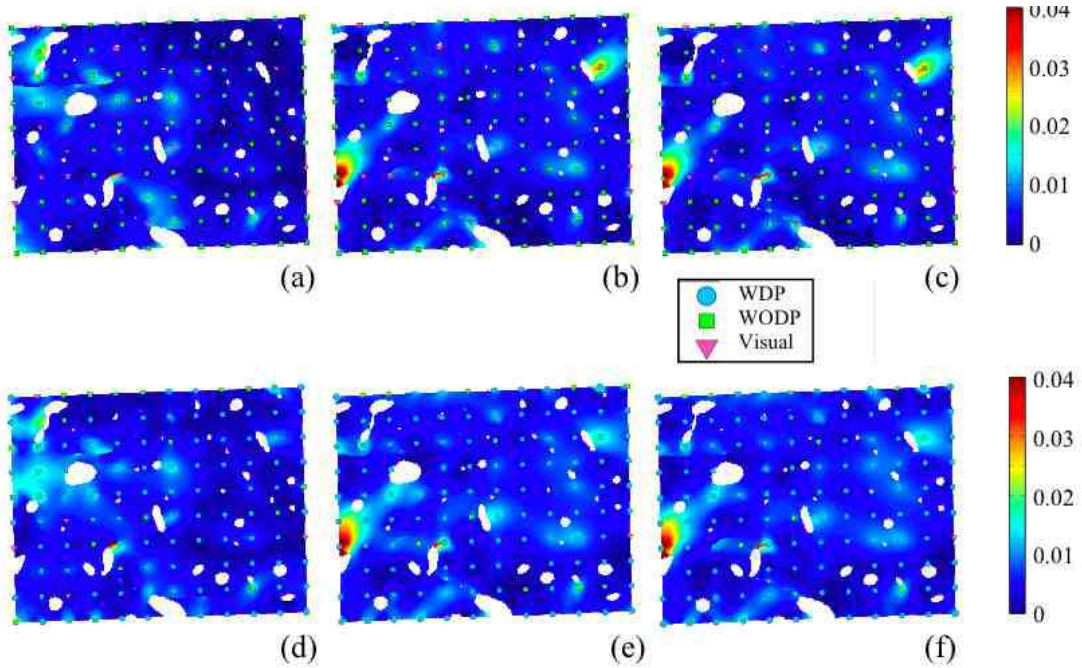

FIG. 4 – Mappings of normalised errors in displacement $N^{fem}_{\Delta\underline{u}_I}$ as defined in Eq. 10 without (WODP) or with (WDP) correlation domain partition in experimental images for (a,d) a direct cross-correlation, (b,e) an invariant gradual cross-correlation and (c,f) a varying gradual cross-correlation. (a-c) relate to a correlation WODP and (d-f) to a correlation WDP.

An average measure of the difference of interpolated fields with respect to a theoretical or visual field are given in Tab. 3 and is further calculated using the L_2-norm denoted $N^{fem}_{\Delta\underline{u}}$ over the microstructure Ω

as follows :

$$N_{\underline{\Delta u}}^{fem} = \sqrt{\frac{\int_{\Omega} \|\underline{\Delta u}^{fem}\|^2 d\Omega}{\int_{\Omega} \|\underline{u}^{fem}\|^2 d\Omega}} \times 100 \tag{11}$$

TAB. 3 – Average normalised interpolated displacement difference $N_{\underline{\Delta u}}^{fem}$ (%).

Method	Direct CC	Invariant Gradual CC	Varying Gradual CC
Simulated	.280	.749	.727
WODP	.562	.698	.708
WDP	.589	.733	.720

4 Conclusions

Efficient image correlation procedures for experimental observations of biological tissues have been studied. The methods focus on how to reliably interpolate information that are sampled at a relevant discrete point set within a large amount of data using FEM. The interpolation approach assumes a local simplified constitutive behavior in the framework of linear elasticity for small deformations when discrete displacements are consistently measured by image correlation on the basis of local homogeneous at a number of points that must be sufficient. The microstructure of Haversian cortical bone has the particularity to contain material discontinuities, holes, interface layers and cracks. The effects of this morphology, in particular cracks and interface layers, have led to consider two different approaches WDP and WODP that partition or not the correlation domain along discontinuities.

For multiple load step experiments, gradual and direct correlations are compared during a four-step DIC analysis of a bone micro-compression test. The overall recognition performance is therefore much higher when using a gradual correlation method than with a direct correlation method, which may be explained by a higher difference in deformation (and therefore a higher variation in grey-level patterns) between two microscopy observations with the direct method. The combination of WODP or WDP correlations complemented by visual measurements that are interpolated by a coherent finite element discretisation in challenging areas make it possible to efficiently measure the displacement field in biological tissues up to 0.93 % precision.

Gradual correlations show fewer displacement discrepancies near cracks even though the accuracy assessment remains difficult in bone where no theoretical field is known and the results could only be compared to single pixel measurements. In experimental images, the normalised value of the overall discrete displacement difference with respect to visual measurements are similar in each WODP or WDP sub-groups and slightly raised in WDP possible by the values calculated near cracks. However after addition of the visual measures at the wrong and few unreliable points in the FEM interpolation, the normalised average interpolated displacement difference is sensibly reduced down to similar values found in simulated images in particular for gradual methods.

Bone micro-compression presented in this study focuses on the analysis of the field near microcracks that appear in large numbers. WDP method appears then as an adequate procedure at the exception of few points within cement lines and that were handled by visual measures.

Références

[1] M. A. Sutton, W. Wolters, W. J. Peters, W. F. Ranson, S. R. McNeill. *Determination of displacements using an improved digital image correlation*, Image and Vision Computing, 1, page 133-page 139, 1983.

[2] P. Doumalin, M. Bornert, J. Crépin. *Characterization of the strain distribution in heterogeneous materials*, Méc Ind, 4, page 607-page 617, 2003.

[3] W. H. Peters, W. F. Ranson, J. F. Kalthoff, S. R. Winkler. *A study of dynamic near-crack-tip fracture parameters by digital image analysis*, Journal de Physique, Colloque C5, page 631-page 638, 1985.

[4] S. R. McNeill, W. H. Peters, M. A. Sutton. *Estimation of stress intensity factor by digital image correlation*, Engineering Fracture Mechanics, 28, page 101-page 112, 1987.

[5] N. Lenoir, M. Bornert, J. Desrues, P. Bésuelle, G. Viggiani. *Volumetric Digital Image Correlation Applied to X-ray Microtomography Images from Triaxial Compression Tests on Argillaceous Rock*, Strain, 43, page 193-page 205, 2007.

[6] A. Germaneau, P. Doumalin, J. C. Dupré. *Full 3D measurement of Strain Field by Scattered Light for Analysis of Structures*, Experimental Mechanics, 47, page 523-page 532, 2007.

[7] T. C. Chu, W. F. Ranson, M. A. Sutton, W. H. Peters. *Applications of Digital-Image-Correlation Techniques to Experimental Mechanics*, Experimental Mechanics, 25(3)), page 232-page 244, 1985.

[8] H. A. Bruck, S. R. McNeill, M. A. Sutton, Peters III, W. H. *Digital Image Correlation Using Newton-Raphson Method of Partial Differential Correction*, Experimental Mechanics, 29(3), page 261-page 267, 1989.

[9] P. Doumalin, M. Bornert, D. Caldemaison. *Microextensometry by Image Correlation Applied to Micromechanical Studies Using the Scanning Electron Microscopy*, Proceedings of the International Conference on Advanced Technology in Experimental Mechanics, Japan Society of Experimental Engineers, page 81-page 86, 1999.

[10] J. Zhang, G. Jin, S. Ma, L. Meng. *Application of an improved subpixel registration algorithm on digital speckle correlation measurement*, Optics and Laser Technology, 35, page 533-page 54, 2003.

[11] D. R. Einstein, A. D. Freed, N. Stander, B, Fata, I. Vesely. *Inverse parameter fitting of biological tissues : a response surface approach*, Annals of Biomedical Engineering, 33(12), page 1819-page 1830, 2005.

[12] M. A. J. Cox, N. J. B. Driessen, R. A. Boerboom, C. V. C. Bouten, F. P. T. Baaijens. *Mechanical characterization of anisotropic planar biological soft tissues usinf finite indentation : experimental feasibility*, Journal of Biomechanics, 41, page 422-page 429, 2008.

[13] P. Seshayier, J. D. Humphrey. *A sub-domain inverse finite element characterization of hyperelastic membranes including soft tissues*, Journal of Biomechanical Engineering, 125, page 363-page 371, 2003.

[14] E. Budyn, T. Hoc. *Analysis of micro fracture in human Haversian cortical bone under transverse tension using Extended Physical Imaging*, International Journal for Numerical Methods in Engineering, 82(8), page 940-page 965, 2009.

[15] P. Doumalin. *Microextensométrie locale par corrélation d'images numériques*, Ph.D Thesis, 2001.